Application of a Model Predictive Control Strategy on a Fluid Catalytic Cracking Pilot Plant

George M. Bollas[1], Simira A. Papadopoulou[2], Angelos A. Lappas[1], Spyros S. Voutetakis[1], Panos Seferlis[1], and Iacovos A. Vasalos[1]

[1] Chemical Process Engineering Research Institute (CPERI), Centre for Research and Technology Hellas (CERTH), 6th km Charilaou–Thermi Rd, PO Box 361, Thessaloniki, GR-570 01, Greece,

[2] Department of Automation, Alexander Technological Educational Institute (ATEI) of Thessaloniki, P.O. Box 14561, Thessaloniki, GR-541 01, Greece

Introduction

Chemical process industry faces the potential of applying model-based predictive control strategies on the fluid catalytic cracking (FCC) unit as a very promising solution for process optimization and profit maximization. However, the cost of developing a reasonably accurate first-principles model for the FCC process is usually prohibitive. This is due to the strong interactions and the high degree of uncertainty in the integrated riser-regenerator loop. The stochastic nature of the air distribution in the regenerator, the moderately defined flow regime of the gas-catalyst mixture in the riser, and the catalyst circulation throughout the unit mainly form a complex integrated system. The different feed and catalyst qualities can be considered as typical disturbances to the system. On the other hand, operational constraints set for safe and stable operation, product specifications and environmental restrictions contribute to the challenges of an already complex control problem.

The main objective of this work was to improve the control performance in the FCC pilot plant (PP) operated in Chemical Process Engineering Research Institute (CPERI - Thessaloniki, Greece). This PP is operated in a mode suitable for catalyst benchmarking experiments. Therefore, there are many similarities and several differences between the operation of the pilot plant and that of a typical industrial unit. While the potential of yielding more market-oriented FCC products, increasing the capacity and the stability are the typical concerns in industrial operation practice, the main concern in the PP process is the stable operation within a narrow process window. Catalysts should be evaluated at constant conversion levels and riser reactor temperatures. Therefore, control of this pilot scale process faces several challenges:

- Riser temperature, controlled by the catalyst circulation rate in the closed loop plant operation, should satisfy a specified set-point that guarantees constant selectivity in the product slate.
- Conversion of the gas-oil feed should meet a determined value for easy comparison (testing) of variable catalyst activity and selectivity.
- Excess gas from the regenerator is subject to environmental constraints regarding the CO, SO_2, NOx emissions in commercial units and this pattern should be followed, or even examined, in the PP operation also.

While the PP unit was operated many years through the application of conventional control schemes based on several PID controllers, unit productivity is related to the stability and ease of operation at specified conditions. A model predictive control (MPC) strategy was therefore implemented for the tight and efficient control of the pilot process. The effective manipulated variables in the PP are the catalyst circulation rate, feed preheat temperature, combustion air flow rate (and temperature), and gas-oil feed flow rate (though in an industrial unit it is driven by the need for target production), while the gas-oil composition and the catalyst quality are considered as disturbances. The interest is in controlling the regenerator and riser temperatures, conversion (feed basis), and coke yield

(feed basis). However, the variables that can be measured online in the PP are the riser and regenerator temperature, the regenerator flue gas, the system pressure and pressure drops. Conversion and coke yield are therefore inferred by the available process measurements and the modeling relations. Thus, it is possible to implement a feedback control scheme that performs optimization through a cost function around the desired operational point. In this scheme constraints on the emissions of the regenerator (CO, NOx, and SO_2) are easily implemented. As the PP regenerator operates under full combustion mode the goal of minimum to zero CO emissions is easily achieved, yet for the other two goals the effect of the optimal operating point of the PP should be explored.

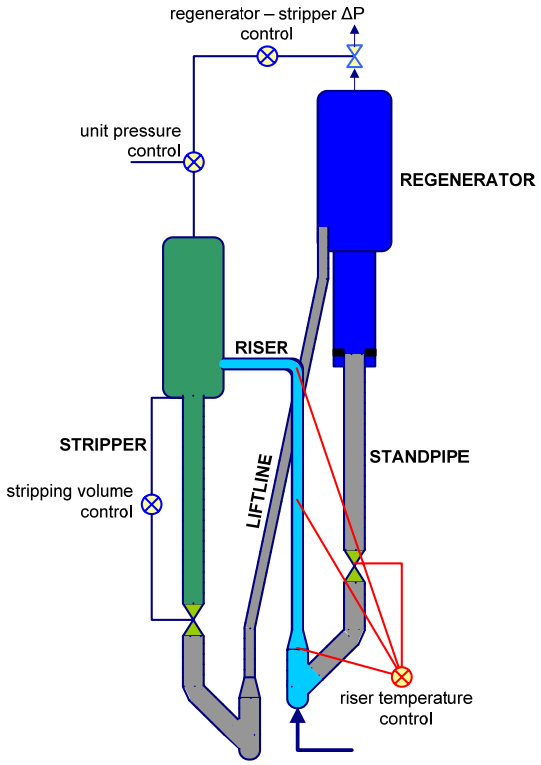

Figure 1. Schematic diagram of the FCC pilot plant.

The development of the control structure underwent two main stages, the simulation study and the implementation to the real process level. The first was done by creating a framework with two instances of the model: an original entity of the simulator, referred to as the "Virtual Process" (VP) and another one in the MPC scheme. A disturbance, such as a change in catalyst quality, was implemented in the VP to test the efficiency and robustness of the MPC. Having chosen and verified the most functional control structure followed by a suitable tuning (e.g., objective function weighting factors) the study resulted to a reliable MPC scheme to be applied on the actual pilot plant. Control parameter updates were obtained using the process measurements and the dynamic model. The optimal piecewise constant future control actions were calculated through dynamic programming over desired prediction and control horizons. The sensitivity of the performance of the online optimal non-linear MPC with respect to the duration of the control intervals and the prediction and control horizons was examined in conjunction to the effort for the numerical solution.

Process description

The FCC pilot plant of CPERI (Figure 1) operates in a fully-circulating mode and consists of a

riser reactor, a fluidized bed regenerator, a stripper and a liftline. The riser reactor operates in pseudo-isothermal plug flow conditions, whereas the regenerator operates in full combustion mode under pseudo-adiabatic conditions. Two slide valves, one at the exit of the regenerator standpipe and one at the exit of the stripper standpipe regulate the catalyst circulation throughout the unit. The regenerator standpipe slide valve manipulates the catalyst circulation to control the riser temperature, whereas the stripper slide valve operates for constant stripper level (i.e. stripping volume). An on-line oxygen analyzer monitors the excess of oxygen and controls the combustion air flow rate. The process pressure, the control valves and the power supply to electrical heaters are controlled by numerous algorithmic PID controllers.

The main task of the PP is catalyst benchmarking. The goal is to maintain the operation within a narrow predefined window in order to achieve standard feed conversion. This practice is especially adopted for gathering comparable results in terms of catalyst selectivity, so any experiment not fulfilling that requirement is useless. In this way, the overall control objective translates to the elimination of repetitive and useless experiments.

Process model

The simulator of the pilot plant includes three main sections: a pseudo-steady state model of the riser reactor, a dynamic model of the regenerator and a set of dynamic and pseudo-steady state models of the stripper, the regenerator standpipe, the liftline and the slide valves. For the specific case of the CPERI pilot plant, the dynamic effects of the riser, the cyclones, the liftline and the regenerator standpipe were assumed negligible, as their operation has a significantly lower impact on the process dynamics, compared to the two large vessels of the plant, the stripper and the regenerator. The residence times of these two units are so much longer that the dynamic effect of the rest is suitably neglected. In both the pilot plant and in a typical commercial unit, the behavior of the regenerator dominates the dynamic and the steady state behavior of the integrated unit [1]. The riser residence times are much shorter compared to those of the regenerator, hence one can, at any instance, describe the riser reactor by a set of pseudo-steady state equations, which simplifies the dynamic analysis. Despite the pseudo-steady state assumption, the riser still affects the unit dynamics. The main impact of the riser operation on the dynamic (and steady state) behavior of the integrated system is through coke production and on heat consumption. That is because the amount of coke on spent catalyst and the catalyst rate entering the regenerator indirectly affect the dynamic behavior. For instance, a decrease on the regenerator temperature will result to a lower temperature stream entering the riser. The temperature drop is compensated by a rise in the catalyst circulation rate. With the catalyst circulation rising, the important side effect is the coke production increase of the riser, which in turn leads to a variation of the regenerator temperature (increase or decrease depending on the regenerator state), which again variably affects the riser and so on. Therefore, the accurate prediction of pseudo-steady state conversion, coke yield and heat of cracking and vaporization is significant, when describing the effect of riser in the integrated dynamic system.

The pseudo-steady state and dynamic sub-models that constitute the dynamic simulator of the PP have been presented in the literature [2-5] and are briefly presented in Appendices I and II. A coupled kinetic-hydro-dynamic model has been developed for the simulation of the pilot riser reactor in pseudo-steady state conditions [4]. The catalyst hold-up and residence time in the reactor were calculated on the basis of empirical hydro-dynamic correlations and the gas-oil conversion and coke yield were predicted through a Blanding type [6] kinetic model. The prediction of gas-oil conversion and coke yield were the only two lumps of the riser sub-model essential for inclusion in the complete simulator, therefore using a more detailed lumped model was futile. The effect of feedstock properties on gas-oil conversion and coke yield was expressed through semi-empirical correlations developed on

the basis of experiments performed with constant catalyst and a variety of feedstocks [3]. The effects of catalyst type and quality were expressed through a "catalyst index" [3]. This means that a different array of indices (one for each product) was assigned to each catalyst to express its activity and selectivity. The pseudo-steady state model of the FCC riser reactor was developed on the basis of the following assumptions:

- the aggregate effects of operating conditions, feed properties and catalyst type on the cracking reactions are simulated by the product of their discrete functions
- the riser reactor is assumed to be running in concurrent plug flow of gas and solids under pseudo-isothermal conditions
- second-order rate apparent kinetics are applied for gas-oil conversion
- catalytic coke deposition parallels catalyst deactivation [7].

The model of the regenerator was based on the two-phase theory of fluidization [8], in which the gas-solids flow is assumed to follow the bubbling bed regime, consisting of two zones: a dense zone at the regenerator bottom comprised by a bubble and an emulsion phase, and a dilute zone at the regenerator top, called the freeboard. The assumptions made for the simulation of each phase [5, 9] are:

- the bubble phase is free of catalyst particles
- plug flow regime is assumed for the bubble phase
- the emulsion phase gas and catalyst particles are assumed fully mixed
- the freeboard is modeled as an ideal plug flow reactor
- the catalyst particles are hydro-dynamically represented by their average size, density and porosity, while the particle size distribution is used for the emulsion to freeboard entrainment rate calculation
- diffusion in the catalyst particles is neglected
- due to the high temperatures in the FCC regenerator, the ideal gas law is valid
- the regenerator reactor is adiabatic.

The model equations were grouped into two main modules that serve for the two main sections of the unit, the riser and the regenerator. A third module was used for the simulation of the stripper and the slide valves, the liftline and the standpipe. The assumptions made for the simulation of the stripper are:

- the stripper is a perfectly mixed reactor in minimum fluidization conditions
- the stripping efficiency of the pilot stripper is 100%.

The dynamic material and energy balance equations form a system of Differential-Algebraic Equations (DAE) that is solved using the equation oriented environment of gPROMS [10]. The dynamic model, the MPC algorithm and the EKF module were merged in a compound module, formed by a gPROMS entity and a MATLAB module communicating through Excel files that serve as the bridge between the two programs.

FCC pilot plant control

Pilot Process Control Objectives

The initial approach presented in this project will focus on improving the control performance of the unit through the manipulation of the riser. That is dictated by the operational conditions of the CPERI pilot regenerator, which allow a small margin for optimization, since the primary target for minimal polluting emissions is in any case achieved through full combustion of the coke under excess air conditions. So, as a first step, the optimal control case will be explored without imposing additional

constraints (minimal CO emissions or specified regenerator temperature) considering the regenerator operation. Still, the regenerator operation significantly interacts with the riser. As mentioned in the previous section, the regenerator defines the dynamics of the unit. MPC optimal control of the riser cannot be achieved via a stand-alone riser model. It requires an integrated accurate model of the riser-regenerator system, mainly due to the fact that both vessels interact with each other through stream recycling. As seen in Figure 1, any variation in the coke/catalyst output stream of the riser is eventually led to the regenerator. The regenerator operation in turn, is notably affected by the transition of the input, resulting in dynamically changing operating conditions and output composition, which are fed back to the riser as a recycle stream affecting it again. It is obvious that the operation of the regenerator must not be neglected and that modeling and monitoring the regenerator is essential for controlling the riser. The effect of the accuracy of the model on the controlling efficiency was extensively discussed in the Model Predictive Control theory [11]. In general, the model of the process should be accurate enough to maintain good prediction properties over the range of operating conditions of interest. The model used for this project has been developed and presented in detail in other relevant publications [2], in which its ability to simulate accurately the dynamics of the PP has been demonstrated.

A robust control system presupposes a suitable choice of the controlled (output) and manipulated (input) variables. The manipulated variables should be the ones that highly affect the unit outputs. Moreover, they must allow for operational flexibility and posses the ability to alleviate the effects of disturbances successfully. The controlled variables should be chosen according to the control objectives (yield maximization, temperature stability etc.). At this point, it is imperative to present a brief degrees of freedom analysis of the system. The riser sub-section is described by 5 basic equations:

$$y_x = f_x\left(\dot{W}_F, \dot{W}_C, \dot{W}_N, P_{\mathrm{RS}}, T_{RX}, p\left(feed\right), p\left(cat\right)\right) \tag{1}$$

$$y_c = f_c\left(\dot{W}_F, \dot{W}_C, \dot{W}_N, P_{\mathrm{RS}}, T_{RX}, p\left(feed\right), p\left(cat\right)\right) \tag{2}$$

$$\begin{aligned}\dot{W}_F \times f_F\left(T_{PR}, T_{RX}, p\left(feed\right)\right) + \dot{W}_C \times f_C\left(T_{D:\mathrm{RG}}^{(t)}, T_{RX}, p\left(cat\right)\right) + \\ \dot{W}_N \times f_N\left(T_{D:\mathrm{RS}}, T_{RX}, p\left(inert\right)\right) + \Delta H_{vap} + \Delta H_{crack} = 0\end{aligned} \tag{3}$$

$$\Delta H_{vap} = \dot{W}_F \times f_v\left(\dot{W}_F, \dot{W}_C, T_{PR}, T_{RX}, T_{D:\mathrm{RS}}, p\left(feed\right)\right) \tag{4}$$

$$\Delta H_{crack} = \dot{W}_F \times f_k\left(y_x, T_{RX}, p\left(feed\right)\right) \tag{5}$$

Practically, the system of eqs.(1) - (5) briefly describes the mass and energy balances of the riser section. More details on those are provided in the Appendices (eq.(14) - (17)). The operational variables (unknowns) occurring above, are 14: the conversion (y_x) and the coke yield (y_c), the feed rate ($\dot{W}_F$) the inert rate ($\dot{W}_N$), the catalyst circulation rate ($\dot{W}_C$), the pressure (P_{RS}) and the temperature (T_{RX}) of the reactor, the feed preheat temperature (T_{PR}), the temperature at the regenerator dense section ($T_{D:\mathrm{RG}}^{(t)}$), the feed vaporization enthalpy (ΔH_{vap}), the energy consumed by the cracking reactions (ΔH_{crack}) and the properties or quality indices of the feed ($p(feed)$), the inert ($p(inert)$) and the catalyst ($p(cat)$). The respective schematic system of equations for the regenerator (neglecting the dynamic clauses of the stripper) are the following:

$$c_{c:\mathrm{RG}}^{(t)} = f_c\left(y_c, \dot{W}_F, \dot{W}_{g:\mathrm{RG}}^{(l_D=0)}, c_{g:\mathrm{RG}}^{(l_D=0)}, c_{g:\mathrm{RG}}^{(l_F=1,\,t)}, c_{c:\mathrm{RG}}^{(t)}, \dot{W}_C, T_{D:\mathrm{RG}}^{(t)}, P_{\mathrm{RG}}\right) \tag{6}$$

$$c_{g:\mathrm{RG}}^{(l_F=1,\,t)} = f_g\left(y_c, \dot{W}_F, \dot{W}_{g:\mathrm{RG}}^{(l_D=0)}, c_{g:\mathrm{RG}}^{(l_D=0)}, c_{g:\mathrm{RG}}^{(l_F=1,\,t)}, c_{c:\mathrm{RG}}^{(t)}, \dot{W}_C, T_{D:\mathrm{RG}}^{(t)}, P_{\mathrm{RG}}, p\left(air\right)\right) \tag{7}$$

$$\dot{W}_C \times f_C\left(T_{RX}, T_{D:\mathrm{RG}}^{(t)}, p\left(cat\right)\right) + \dot{W}_{g:\mathrm{RG}}^{(l_D=0)} \times f_g\left(T_{g:\mathrm{RG}}^{(l_D=0)}, T_{D:\mathrm{RG}}^{(t)}, T_{F:\mathrm{RG}}^{(l_F=1)}, p\left(air\right)\right) + \Delta H_{comb} = 0 \tag{8}$$

$$\Delta H_{comb} = f_r\left(y_c, \dot{W}_F, W_{g:\mathrm{RG}}^{(l_D=0)}, \dot{W}_C, T_{g:\mathrm{RG}}^{(l_D=0)}, T_{D:\mathrm{RG}}^{(t)}, T_{F:\mathrm{RG}}^{(l_F=1)}, P_{\mathrm{RG}}, p\left(air\right)\right) \quad (9)$$

The system of eqs.(6) - (9) describe very briefly the extended system of equations of the regenerator. The variables appearing here are 8: the air (for combustion) flow rate at the bottom of the regenerator ($\dot{W}_{g:\mathrm{RG}}^{(l_D=0)}$), the composition of the gas exiting from the regenerator top ($c_{g:\mathrm{RG}}^{(l_F=1,\,t)}$), the composition of coke on the regenerated catalyst ($c_{c:\mathrm{RG}}^{(t)}$), the average regenerator pressure (P_{RG}), the inlet temperature of the combustion air ($T_{g:\mathrm{RG}}^{(l_D=0)}$), the heat of the exothermic reactions (ΔH_{comb}) the combustion air composition ($c_{g:\mathrm{RG}}^{(l_D=0)}$) and its properties ($p(air)$). The system in its general form totals 22 variables and 9 equations, therefore 13 degrees of freedom. It is noted that the analysis presented, despite the generalities, requires full comprehension of the FCC unit operation and it can be easily adopted by any pilot or industrial unit.

The 13 independent variables of the FCC operation are described below: the feed rate, the inert rate, the riser pressure, the catalyst circulation rate, the feed preheat temperature and the qualities of the feed, the inert and the catalyst for the riser section. For the regenerator they are the air rate at the bottom, the pressure and the inlet air temperature, composition and properties. In a typical industrial unit: 1) the feed rate is set to meet the maximum capacity of the unit, 2) the inert rate and 3) the inert quality follow a predefined pattern in order to retain constant partial pressure of the hydrocarbons in the riser, 4) the temperature, 5) the composition and 6) the properties of the combustion air are constant. These bounds are also followed in PP operation, although not always for the same reasons. Moreover, specifically in the pilot plant: 7) the combustion air rate of the pilot regenerator is controlled separately in order to satisfy the low emissions criterion. Also, 8) the feed quality and 9) the catalyst quality are considered as unknown disturbances. The reason for the latter is their stochastic nature in industry, meaning that the feed quality description is usually unavailable, because it is a mixture of various refinery streams and the catalyst quality is changing perpetually due to the continuous addition of a small amount of fresh catalyst. Furthermore, feed or/and catalyst qualities are the usual unknowns during PP benchmarking experiments. Provided that 10) the riser pressure and 11) the regenerator pressure are controlled by separate subsystems, the only independent variables suitable for manipulation in the PP, for the purpose of benchmarking experiments, are the catalyst circulation rate and the feed preheat temperature.

The main objective in both the pilot plant and the industry FCC process is the optimization of the riser conversion on feed basis, while maintaining the riser temperature around a set point, which guarantees the constant effect of operating conditions on product selectivity. In industry the conversion control targets maximum profitability. In the PP, where the intention is the efficient catalyst benchmarking, the interest lays in maintaining the operation within a predefined span. The riser conversion, the riser temperature, the feed preheat temperature and the catalyst circulation rate are interrelated variables and comprise a system of equations (eqs.(1) - (5)), which under stable operation is uniquely defined (within the narrow bounds of the PP operation). The manipulated catalyst circulation rate obviously affects the conversion, but it also affects the heat build-up, consumption and loss of the system so it has an impact on the riser temperature. Riser temperature and riser conversion are correlated. This implies that for a given value of the riser temperature, conversion is defined uniquely and vice-versa (given that every other input variable of the riser is constant). The last fact provides two alternatives for the control problem: If riser conversion measurements were available then it might be directly controlled by manipulating the catalyst rate and feed preheat. In the most usual case that the riser temperature measurement is more accessible and no conversion measurement is available online, then conversion control can be performed using an inferred value calculated by eq.(1).

On the basis of the above analysis, an MPC strategy can be implemented for the control of conversion on feed basis and riser temperature through the proper manipulation of the catalyst circulation rate and the feed preheat temperature. This strategy should lead to the direct targeting of the desired conversion and reduce the number of required experiments with the same catalyst in catalyst evaluation tests.

MPC principles

Model predictive control is based on the fact that past and present control actions affect the future response of the process [11]. Having selected a time horizon extending into the future, the prediction of the process model is calculated, based on past control actions. The response of the model can then be compared to a desired trajectory if no further control actions are to be taken. The variation between the desired control trajectory and the predictions can therefore be minimized, through the calculation of a specified number of future control actions (Figure 2). The control horizon (i.e. the period for which future control actions are calculated) may be selected smaller or equal to the prediction time horizon, during which the comparison of the desired to the predicted trajectories is performed. At each time interval the first optimal control action in the calculated sequence is implemented and a new measurement of the actual response of the process is obtained. The model-based predictive control principles are presented in Figure 2.

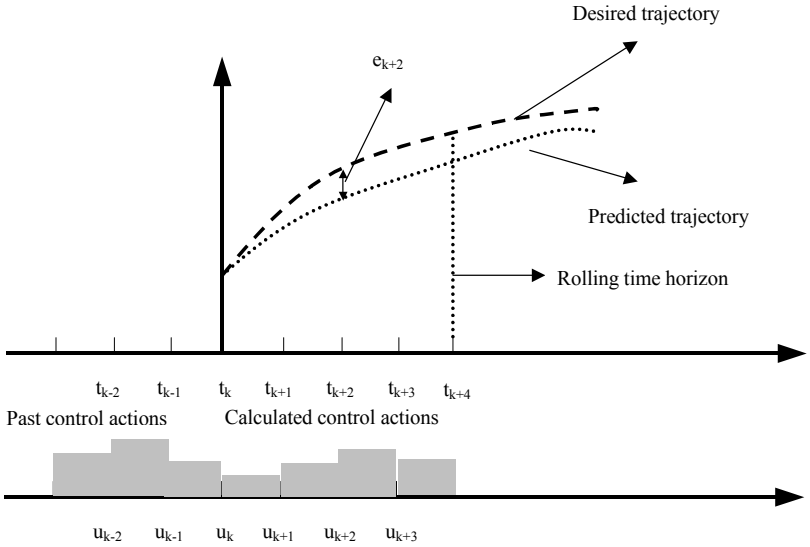

Figure 2. Schematic representation of the principles in model-predictive control.

The deviation of the model prediction from the actual response of the process is recorded and considered as the error of the process model, as shown in the block diagram of the MPC system (Figure 3). The calculated error defines a bias term that is used to correct the future predictions of the model. The bias model term encompasses contributions from model mismatch, unmeasured disturbances, and measurement error. It is assumed that this error would be persistent for the entire prediction horizon. Thus, error feedback is maintained in the control system allowing integral action and elimination of steady-state offset. The block diagram describing the system is presented in Figure 3.

A parameter and state estimator can be added to enhance the model accuracy and the overall MPC robustness. For non-linear systems robust state and parameter estimation can be achieved through the use of an Extended Kalman Filter (EKF). The correction of the model parameters and its states leads to the gradual minimization of the model - process mismatch.

The formulation of the control problem results in a dynamic program. The objective function contains the integral of the squared error of the controlled variables from the desired trajectory, a move suppression factor on the manipulated variables that penalizes high values in the rate of change for the control actions and a steady state optimality factor for restricting the range of the possible solution within the operational limits. The behavior of the manipulated variables is considered as a sequence of piecewise values that minimize the objective function. The prediction and control horizons are divided in equally spaced time intervals, during which the manipulated variables remain constant. Upper and lower bounds apply for the manipulated variables along the control horizon, as required by the physical limitation of the system (e.g., $\dot{W}_C$ cannot exceed its value for the respective maximum available valve opening or the minimum flow necessary for safe operation). The solution method involves successive iterations between the optimizer, that evaluates the optimal values of the manipulated variables, and the integrator, that calculates the dynamic response of the system and the sensitivity of the control actions to the control objectives. Variable bounds and path constraints are considered for violation along the optimal control path.

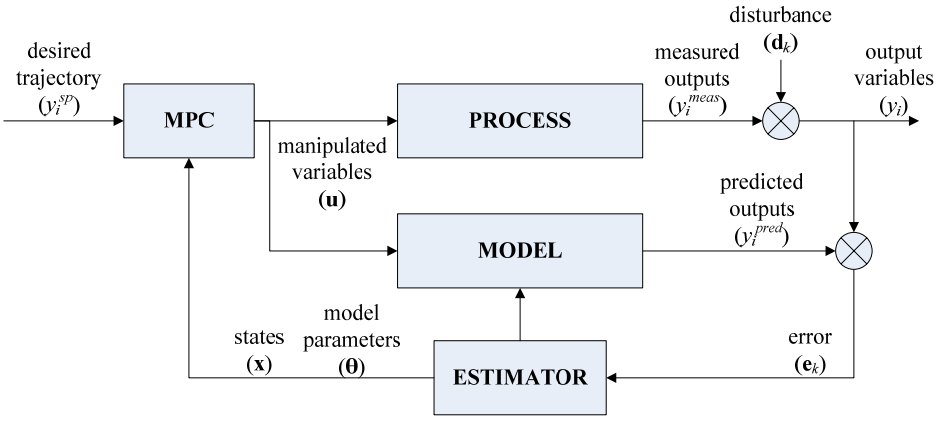

Figure 3. Control block diagram of the process.

The mathematical representation of the model-based predictive control algorithm is given by the following expression:

$$\min_{\mathbf{u}_{k+j-1}} \mathrm{J}_{MPC} = \sum_{j=1}^{N_P} \left\| \hat{\mathbf{y}}_{k+j} - \mathbf{y}_{k+j}^{sp} \right\|_{\mathbf{w}_{k+j}^{y}}^{2} + \sum_{j=1}^{N_C} \left\| \Delta \mathbf{u}_{k+j-1} \right\|_{\mathbf{w}_{k+j-1}^{\Delta u}}^{2} + \sum_{j=1}^{N_C} \left\| \mathbf{u}_{k+j-1} - \mathbf{u}_{k+j-1}^{ss} \right\|_{\mathbf{w}_{k+j-1}^{u}}^{2}$$

subject to:

$$\begin{aligned} &\dot{\mathbf{x}} = \mathbf{f}\left(\mathbf{x}, \mathbf{u}\right) \\ &\mathbf{y} = \mathbf{g}\left(\mathbf{x}, \mathbf{u}\right) \\ &\mathbf{e}_{k+j-1} = \left(\mathbf{y}^{meas} - \mathbf{y}^{pred}\right)_{k+j-1} \\ &\hat{\mathbf{y}}_{k+j} = \mathbf{y}_{k+j}^{pred} + \mathbf{e}_{k+j-1} \\ &\mathbf{u}^{l} \le \mathbf{u}_{k+j-1} \le \mathbf{u}^{u} \\ &N_C = \left(T_C - T_k\right) / \Delta t_C,\ N_P = \left(T_P - T_k\right) / \Delta t_P \end{aligned} \tag{10}$$

where **x**, **u**, **y** denote the vectors of the state, manipulated (i.e. control actions) and output variables of the system, respectively. Symbols **f** and **g** denote the sets of differential and algebraic model equations. Vector $\hat{\mathbf{y}}$ denotes the predictions for the system output variables that include the contribution of the

bias term on the model predictions. Vector $\mathbf{y}^{sp}$ denotes the desired response (set point) of the system output variables. Vector $\mathbf{e}_k$ denotes the difference between the measured output variables $\mathbf{y}^{meas}$ and the predicted values $\mathbf{y}^{pred}$ at time instant k. The current formulation assumes that the error on the predictions will persist and remain constant for the entire length of the prediction time horizon. T_P and T_C denote the prediction and control horizons, reached through N_P and N_C time intervals, respectively. The tuning parameters of the controller are the weights $\mathbf{w}^y$, $\mathbf{w}^u$ and $\mathbf{w}^{\Delta u}$, and the length of the prediction and control horizons. A long prediction horizon allows the control scheme to compensate for slower dynamics that affect the response of the system further into time. However, large prediction horizons make the control scheme more susceptible to unmeasured disturbances. On the other hand, a short control horizon may lead to aggressive control actions, as the controller attempts to correct the trajectory with a few moves through short time period.

Extended Kalman Filter

The model states, $\mathbf{x}$, and parameters, $\boldsymbol{\theta}$, are updated every time a new set of measurements becomes available. Therefore, an Extended Kalman Filter (EKF) is utilized due to the nonlinear nature of the process model. The dynamic process model is linearized and brought to its equivalent state space representation. The deterministic process states, $\mathbf{x}^{\mathbf{d}}$, as defined by the process balance equations are augmented with stochastic states, $\mathbf{x}^{\mathbf{s}}$, that account for the model parameters and process disturbances. These additional states may vary with time in some stochastic manner. Since the functional relationship $\mathbf{f}^{\mathbf{s}}$ for the stochastic state variables is rarely known, the most common assumption, provided that $\mathbf{x}^{\mathbf{s}}$ does not change considerably with time, is to be set equal to a zero vector. Thus, the dynamic behavior of the stochastic state variables is usually modeled as a random walk process. The inclusion of meaningful and consistent non-stationary stochastic state variables, $\mathbf{x}_{\mathbf{k}}^{\mathbf{s}}$, into the state/parameter estimator can eliminate the bias between the mathematical model and the actual process and provide good and unbiased state estimates [12-15].

Hence, the augmented state space model representation is as follows:

$$\begin{aligned} \mathbf{x}_k &= \Phi\mathbf{x}_{k-1} + \Gamma\mathbf{u}_{k-1} + \Xi\mathbf{w}_k \\ \mathbf{y}_k &= \mathrm{H}\mathbf{x}_k + \Delta\mathbf{u}_k + \Lambda\mathbf{v}_k \end{aligned} \tag{11}$$

where $\mathbf{x}_{\mathbf{k}}$ is the entire state vector, $\mathbf{x}_k = \begin{bmatrix} \mathbf{x}_k^d \\ \mathbf{x}_k^s \end{bmatrix}$. $\mathbf{w}_k = \begin{bmatrix} \mathbf{w}_k^d \\ \mathbf{w}_k^s \end{bmatrix}$ and $\mathbf{v}_k$ denote the process and measurement noise, respectively. Process and measurement noise are assumed to behave as zero mean Gaussian shocks with covariance matrices $\mathbf{Q}$ and $\mathbf{R}$, respectively. Matrix $\boldsymbol{\Phi}_{\mathbf{k}}$ denotes the Jacobian of the system with respect to the states and is given by: $\Phi_k = \begin{bmatrix} \Phi_k^{\mathbf{d}} & \Phi_k^{\mathbf{s}} \\ \mathbf{0} & \mathbf{I} \end{bmatrix}$

When a new observation becomes available, the states are updated according to the following equation:

$$\mathbf{x}_{k+1/k+1} = \mathbf{x}_{k+1/k} + \mathbf{K}_k \left\{ \mathbf{y}_{k+1} - \mathrm{H}\left(\mathbf{x}_{k+1/k}\right) \right\} \tag{12}$$

$\mathbf{K}_k$ is the Kalman gain at time t_k computed recursively from the resulting Riccati equations. For increased accuracy of the EKF the process model is linearized in each time interval.

Results

Model-based predictive control of FCC reactor (simulated results)

At this point, it is needed to clarify that, as the catalyst effect on the system can not be modeled, it has been represented by indices [3]. That is, the effects of catalyst type and quality were

expressed through an array of indices (one for each product) that was assigned to each catalyst to express its activity and selectivity. These indices are the unknowns or "constant disturbances" in the PP control problem formulation. The model predictive controller was initially tested on a simulated case study. The MPC framework includes two instances of the model that were concurrently executed. The first instance, which represented the "Virtual Process" or "Virtual Plant" (VP), was depicted by a flawless version of the model. The second introduced a case study including significant amount of mismatch in the reaction kinetics in order to simulate a fictitious simulated process and was used to represent the "Simulator". Hence, in the following the expression "Virtual Process" or VP denotes the process, for which the flawless version of the model was used, and the expression "Simulator" denotes the model with the different kinetic constants. This case study actually included what is expected to be the control problem in the real pilot process level. More specifically, different indices that describe the effect of catalyst activity and selectivity on feed conversion and coke yield have been used in the VP model and the Simulator model. The indices used were those of real catalysts, different for each case (VP and Simulator) taken from the PP experimental database. With this structure the equivalent of a typical catalyst benchmarking experiment was fully reconstructed. The intervals for the control actions (i.e. manipulation of variables) were chosen equal to 2 minutes. The Simulator was updated using infrequent rate process measurement of the reactor temperature and the inferred conversion of the VP. The optimal piecewise constant future control actions were calculated through dynamic programming over the desired prediction and control horizons.

Validation of the model-based predictive control scheme

The different catalyst activity and selectivity between the Virtual Plant and the Simulator act as a constant disturbance in the process cycle. The goal for the MPC was to move the plant operation through a sequence of corrective control actions to the desired level of feed conversion and riser temperature. The following performance index was used:

$$J_k = \sum_{i=1}^{n^y} w_i^y \int_{t_k}^{t_{k+1}} \left(1 - \frac{\hat{y}_i(t)}{y_i^{sp}}\right)^2 + \sum_{i=1}^{n^u} w_i^{\Delta u} \left(\Delta \hat{u}_i\left(t_{k/k-1}\right)\right)^2 + \sum_{i=1}^{n^u} w_i^u \left(1 - \frac{\hat{u}_i(t_k)}{u_i^{ss}}\right)^2 \quad (13)$$

where $\hat{y}_i$ denotes the predictions of the respective variables *i* that incorporate the model prognosis and the error correction (i.e. difference between the measurement and the prediction at the previous time period) and y_i^{sp} the set points of the controlled variables. The second term of eq.(13) denotes the move suppression factor, which penalizes abrupt changes in the manipulated variables. The last term denotes the steady state optimality factor and it aims to drive the MPC actions towards a potentially desired solution, dictated by the plant optimization decision level. Weights *w* express the relative significance of each term in the performance index.

The prediction (N_P) and control (N_C) horizons were selected equal to 20 and 10 minutes, respectively. The length of the prediction horizon is close to the time necessary for the PP to reach the new steady state after imposing a typical change. The length of the control horizon was mainly driven by the computational time for solution that should be lower than the unit sampling interval. The control profile was considered as piecewise constant with the manipulated variables changing every 2 minutes. The length between two consecutive control actions (Δt_C) was chosen on the basis of the frequency of the available measurements. A new optimal sequence of 5 control actions was calculated every 2 minutes. This means that every 2 minutes a new control action was implemented and a new measurement was recorded. The time between two successive measurements was determined considering also the limitation imposed from the computation time required for the solution of the dynamic optimization and simulation of the process model. At each time interval the dynamic non-

linear model was linearized and the EKF was applied. In the linearization the catalyst indices were considered as manipulated variables and then added to the linearized state vector.

The control problem, as posed above, was tested on a simulation environment, in which different catalyst indices ($p(cat)$) were used for the Virtual Process and the Simulator. The indices of a catalyst with higher activity and selectivity and much higher coke selectivity were used in the VP. Moreover, the non-catalytic coke yield, which is a result of the feedstock quality and can be predicted by the model, was intentionally considered different between the PP and the Simulator. In the VP a higher non-catalytic coke yield was used. This was done to examine the performance of the MPC scheme to a disturbance that is not filtered by the EKF. Finally, noise was added to the VP measurements to test the EKF efficiency. These significant differences caused an increase in the feed conversion of the VP and lower riser temperature, compared to those predicted by the Simulator. The task for the MPC algorithm was to lead the VP to the desired conversion ($y_x^{sp} = 65$ %wt) and riser temperature ($T_{RX}^{sp} = 526.7$ °C) under the influence of the disturbances introduced. The bias term (e_k of eq.(10)) (also referred as constant additive disturbance [16]) and the parameter estimation through the EKF were used for improving the Simulator accuracy.

As shown in Figure 4, the VP initiated at 2% higher feed conversion than the desired one and riser temperature 2°C above its set point. The first action of the MPC was to lower the catalyst circulation rate and increase the feed preheat temperature, as dictated by the solution of the dynamic problem. The lower catalyst circulation rate led to lower coke yield (on feed basis), but higher overall ratio of coke rate over catalyst rate entering the regenerator. The latter resulted in increasing the regenerator temperature (Figure 4(f)) and eventually the riser temperature (Figure 4(d)). As the controlled variables are variables of the riser, which operates in pseudo-steady state, the MPC led the process very close to the desired set-points rapidly. Thereafter, using the information of the prediction horizon waited for the dynamics of the process, while making small control actions to compensate for the VP - Simulator mismatch. In Figures 4(g) and (h) it is evident that the regenerator flue gas is not significantly influenced by the sequence of control actions, because of the large excess air supply. The operation in full combustion mode is the reason for the practically zilch CO and the very low SO_2 emissions. Overall, the MPC structure presented promises the establishment of the desired steady state within 40 min, which is very important for the pilot plant operation.

The control loop was continued for a period of 40 min. In the final steady state both the feed conversion and the riser temperature criteria were fully satisfied. The results with the use of the EKF are also presented in Figure 4. It is evident that the EKF was able to absorb the artificial noise introduced and to correct the model predictions. The steady state offset of the filtered model predictions is owed to the feed quality disturbance implemented, which was not filtered. Overall, the MPC structure presented promises the establishment of the desired steady state within 40 min, which is very important for the PP operation.

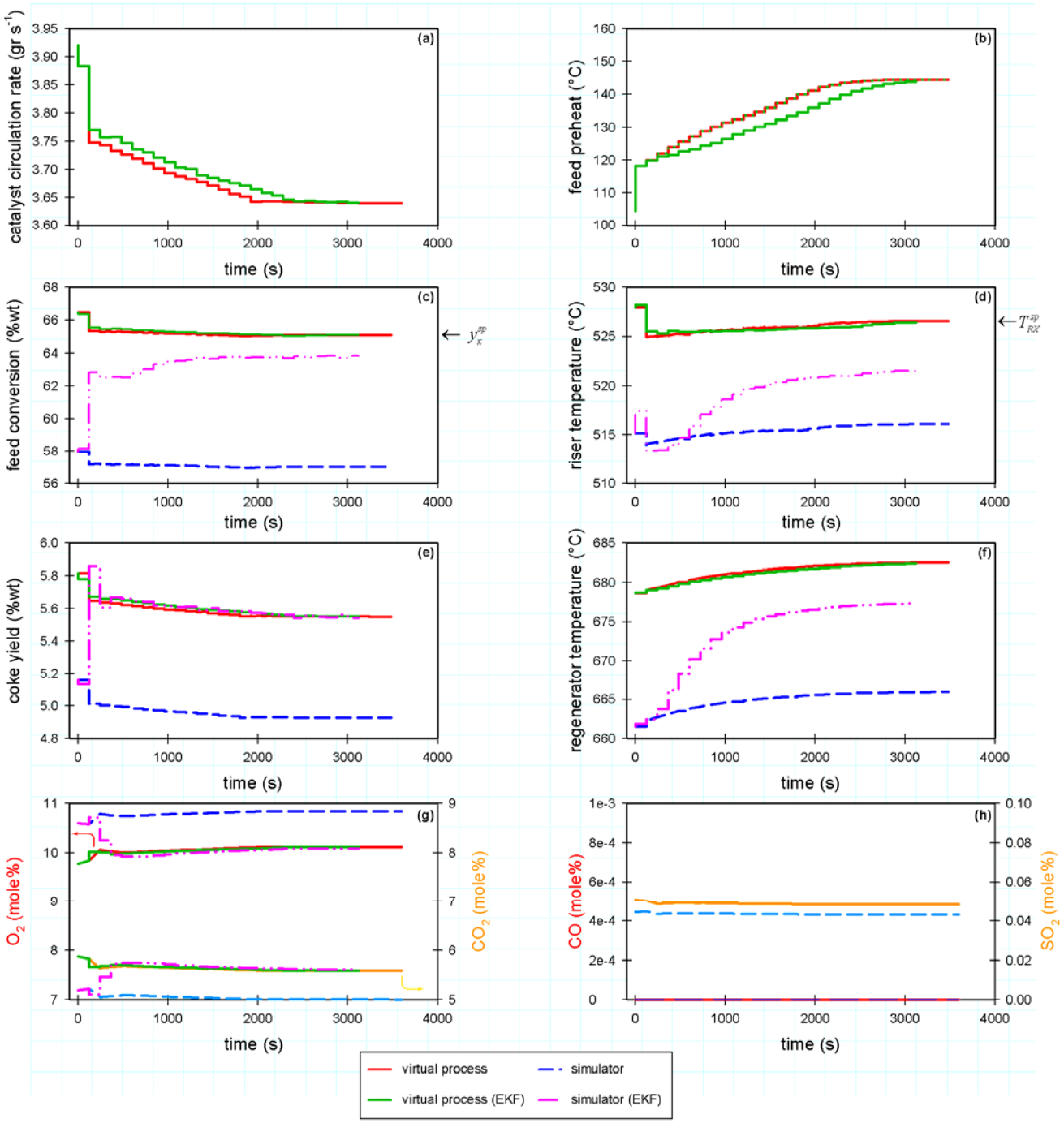

Figure 4. Results of the application of the MPC structure on a simulation environment (continuous lines denote the "Virtual Process" and dotted lines the "Simulator").

Conclusions

An advanced model predictive control strategy that calculates the optimal sequence of manipulated variables over a specified control horizon has been implemented in a pilot- sized FCC unit used for catalyst experimentation. The implementation of the MPC scheme showed extreme robustness to changes in the catalyst activity and selectivity. The MPC scheme allowed for an accurate targeting of the desired feed conversion with little knowledge about the catalyst properties and selectivity. In

conclusion, the MPC strategy allowed for tight following of the prescribed operating conditions and the elimination of additional and/or repeat experiments with the same catalyst in catalyst evaluation tests, thus improving the overall productivity of the catalyst evaluation studies task that the pilot plant is mainly used for.

Acknowledgment

Financial support by the European Social Fund & National Resources - EPEAEK II – ARCHIMEDES is gratefully acknowledged.

Referencess

1. Arbel, A., Huang, Z. P., Rinard, I. H., Shinnar, R. & Sapre, A. V. (1995) Dynamics and control of Fluidized Catalytic Crackers. 1. Modeling of the current generation of FCCs. *Industrial & Engineering Chemistry Research,* 34**,** 1228-1243.
2. Bollas, G. M., Vasalos, I. A., Lappas, A. A., Iatridis, D. K., Voutetakis, S. S. & A., Papadopoulou S. (2006) Integrated FCC Riser - Regenerator Dynamics studied in a Fluid Catalytic Cracking Pilot Plant. *Chemical Engineering Science,* submitted for publication.
3. Bollas, G. M., Vasalos, I. A., Lappas, A. A., Iatridis, D. K. & Tsioni, G. K. (2004) Bulk Molecular Characterization Approach for the simulation of FCC feedstocks. *Industrial & Engineering Chemistry Research,* 43**,** 3270-3281.
4. Bollas, G. M., Vasalos, I. A., Lappas, A. A. & Iatridis, D. (2002) Modeling small-diameter FCC riser reactors. A hydrodynamic and kinetic approach. *Industrial & Engineering Chemistry Research,* 41**,** 5410-5419.
5. Faltsi-Saravelou, O. & Vasalos, I. A. (1991) Fbsim - A model for fluidized-bed simulation. 1. Dynamic modeling of an adiabatic reacting system of small gas-fluidized particles. *Computers & Chemical Engineering,* 15**,** 639-646.
6. Blanding, F.H. (1953) Reaction rates in the catalytic cracking of petroleum. *Industrial & Engineering Chemistry,* 45**,** 1186.
7. Voorhies, A. (1945) Carbon formation on catalytic cracking. *Industrial & Engineering Chemistry,* 37**,** 4.
8. Davidson, J.F., Clift, R. & Harrison, D. (1985) *Fluidization,* London, Academic Press Inc.
9. Faltsi-Saravelou, O., Vasalos, I. A. & Dimogiorgas, G. (1991) Fbsim - A model for fluidized-bed simulation. 2. Simulation of an industrial fluidized catalytic cracking regenerator. *Computers & Chemical Engineering,* 15**,** 647-656.
10. Process Systems Enterprise, (P.S.E.) (2004) gPROMS Advanced User's Guide. London, UK.
11. Marlin, T. E. (1995) *Process Control: Designing Processes and Control Systems for Dynamic Performance,* New York, McGraw-Hill Inc.
12. De Valliere, P. & Bonvin, D. (1990) Application of estimation techniques to batch reactors III. Modelling refinements which improve the quality of state and parameter estimation. *Computers & Chemical Engineering,* 14**,** 799.
13. Gagnon, L. & Macgregor, J. F. (1991) State Estimation for continuous emulsion polymerization. *Canadian Journal of Chemical Engineering,* 69**,** 648.
14. Kozub, D. J. & Macgregor, J. F. (1992) State estimation for semi-batch polymerization reactors. *chemical Engineering Science,* 47**,** 1047.
15. Valappil, J. & Georgakis, C. (2000) Systematic estimation of state noise statistics for extended Kalman filters. *AIChE Journal,* 46**,** 292-308.
16. Nagy, Z. K., Roman, R., Agachi, S. P. & Allgoewer, F. (2005) A real-time approach for moving horizon estimation based nonlinear model predictive control of a fluid catalytic

cracking unit. *7th World Congress of Chemical Engineering, GLASGOW2005, incorporating the 5th European Congress of Chemical Engineering.*
17. Kesler, M. G. & Lee, B. I. (1976) Improve prediction of enthalpy of fractions. *Hydrocarbon Processing,* 55**,** 153-158.
18. Kunii, D. & Levenspiel, O. (1977) *Fluidization Engineering,* Florida, Robert E. Krieger Publishing Company Inc.
19. Richardson, J. F. & Zaki, W. N. (1954) Sedimentation and Fluidization. I. *Transactions of the Institution of Chemical Engineers,* 32**,** 35.
20. Pugsley, T. S. & Berruti, F. (1996) A predictive hydrodynamic model for circulating fluidized bed risers. *Powder Technology,* 89**,** 57-69.
21. Abrahamsen, A. R. & Geldart, D. (1980) Behaviour of gas-fluidized beds of fine powders, part I. Homogeneous expansion. *Powder Technology,* 26**,** 35-46.
22. Geldart, D. (1985) Elutriation. IN Davidson, J. F., Clift, R. & Harrison, D. (Eds.) *Fluidization.* London, Academic Press Inc.
23. Patience, G. S., Chaouki, J., Berruti, F. & Wong, R. (1992) Scaling considerations for circulating fluidized bed risers. *Powder Technology,* 72**,** 31-37.
24. Judd, M. Robin & Dixon, Patrick D. (1978) Flow of fine, dense solids down a vertical standpipe. *AIChE Symp Ser,* 74**,** 38-44.

APPENDIX I: Mathematical Model Formulation

Simulation of Riser

On the basis of the assumptions mentioned above and after integration and rearrangement of the corresponding spatial equations eqs.(14) and (15) were formulated:

$$0 = C\left(catalyst\ type\right)F\left(feed\ quality\right)\frac{k_x}{WHSV}\exp\left(\frac{-E_x}{R_g T_{RX}}\right){t_{C:\mathrm{RS}}}^{n_x} - \frac{y_x}{100-y_x} \tag{14}$$

$$0 = C_c\left(catalyst\ type\right)F_c\left(feed\ quality\right)\frac{k_c}{WHSV}\exp\left(\frac{-E_c}{R_g T_{RX}}\right){t_{C:\mathrm{RS}}}^{n_c} - y_{c_x} \tag{15}$$

The main contributors to the overall enthalpy balance in an FCC plant are the enthalpy of cracking ΔH_{crack}; the enthalpy of vaporization of the gas-oil feedstock; and the enthalpy content of various process streams (gas-oil, catalyst, cracked products, inerts), as shown in eq.(16):

$$0 = \Delta H_{crack} + \Delta H_{vap} + \Delta H_{gas\text{-}oil} + \Delta H_{cat} + \Delta H_{Loss} \tag{16}$$

The enthalpy content of gas-oil vapors was estimated by integration of the empirical correlation of Kesler and Lee [17]. The heat of cracking was estimated as a function of conversion, riser temperature and gas-oil molecular weight, as shown in eq.(17):

$$0 = \ln\left(\frac{x}{100-x}\right)\left(a_1 T_{RX} + a_2 {T_{RX}}^2 + a_3 MW_F\right) + \left(b_1 T_{RX} + b_2 {T_{RX}}^2 + b_3 MW_F\right) - \Delta H_{crack} \tag{17}$$

Simulation of Regenerator

The dense bed volume was calculated on the basis of the overall regenerator dynamics:

$$\frac{dV_{D:\mathrm{RG}}}{dt} = \frac{\dot{W}_{C:\mathrm{RG}}^{(l_D=1)} - \dot{W}_{C:\mathrm{RG}}^{(l_D=0)} + \dot{W}_{C:\mathrm{CY}}^{(l_F=1)} - \dot{W}_{C:\mathrm{CY}}^{(l_F=0)}}{\rho_p\left(1-\varepsilon_e\right)f_e} \tag{18}$$

The material balance for gas components in the bubble phase is:

$$\frac{1}{V_{D:\mathrm{RG}}}\frac{dF_{ib}}{dl_D} = -K_{Mi} + f_b \sum_j^{\text{homo}} a_{ij} K_{Rjb} \tag{19}$$

The energy balance in the bubble phase is given by eq.(20):

$$\frac{1}{V_{D:\mathrm{RG}}}\frac{dQ_b}{dl_D} = -K_H + f_b \sum_j^{\text{homo}} \left(-\Delta H_{Rj}\right) K_{Rjb} \tag{20}$$

In the emulsion phase the material balance equations were formulated separately for gas and solids components, as shown in eqs.(21) and (22) respectively:

$$f_e \varepsilon_e \frac{dc_{ie}}{dt} = \frac{\dot{W}_{ge}^{(l_D=0)}}{\rho_{ge}} \frac{c_{ie}^{(l_D=0)} - c_{ie}}{V_{D:\mathrm{RG}}} + \int_0^1 K_{Mi} dl_D + f_e \varepsilon_e \sum_j^{homo} a_{ij} K_{Rje} + f_e \left(1-\varepsilon_e\right) \sum_j^{hete} a_{ij} K_{Rje} \tag{21}$$

$$f_e \left(1-\varepsilon_e\right) \frac{dc_{ie}}{dt} = \frac{\dot{W}_{C:\mathrm{RG}}^{(l_D=1)}}{\rho_p} \frac{c_{ie}^{(l_D=1)} - c_{ie}}{V_{D:\mathrm{RG}}} + \frac{\dot{W}_{C:\mathrm{CY}}^{(l_F=1)}}{\rho_p} \frac{c_{if}^{(l_F=1)} - c_{ie}}{V_{D:\mathrm{RG}}} + f_e \left(1-\varepsilon_e\right) \sum_j^{hete} a_{ij} K_{Rje} \tag{22}$$

The energy balance equation in the emulsion phase is given by eq.(23):

$$\begin{aligned} &\left(f_e \left(1-\varepsilon_e\right) \sum_i^{solids} c_{ie} cp_{ie} + f_e \varepsilon_e \sum_i^{gas} c_{ie} cp_{ie} \right) \frac{d\left(V_{D:\mathrm{RG}} T_e\right)}{dt} = Q_{C:\mathrm{RG}}^{(l_D=1)} - Q_{C:\mathrm{RG}}^{(l_D=0)} + Q_{C:\mathrm{CY}}^{(l_F=1)} - Q_{C:\mathrm{CY}}^{(l_F=0)} + Q_{ge}^{(l_D=0)} \\ &- Q_{ge}^{(l_D=1)} - Q_{loss} + V_{D:\mathrm{RG}} \int_0^1 K_H dl_D + f_e \varepsilon_e V_{D:\mathrm{RG}} \sum_j^{homo} \left(-\Delta H_{Rj}\right) K_{Rje} + f_e \left(1-\varepsilon_e\right) V_{D:\mathrm{RG}} \sum_j^{hete} \left(-\Delta H_{Rj}\right) K_{Rje} \end{aligned} \tag{23}$$

The superficial bubble gas velocity for the dimensionless fraction of dense bed height l_D, is evaluated by differentiating the ideal gas law in terms of the bubble enthalpy rate term:

$$\frac{du_{gb}}{dl_D} = \frac{R_g}{A_{D:\mathrm{RG}} P_{D:\mathrm{RG}} \overline{cp}_{gb}} \frac{dQ_b}{dl_D} \tag{24}$$

The bubble-emulsion mass interchange K_{Mi} and the heat interchange K_H and the emulsion fraction f_e are evaluated by eqs. (25) - (27), respectively:

$$0 = K_{ti} \left(\frac{F_{ib}}{u_{gb} A_{D:\mathrm{RG}}} - c_{ie} \right) - K_{Mi} \tag{25}$$

$$0 = H_t \left(T_b - T_e\right) - K_H \tag{26}$$

$$f_e = \int_0^1 \left(1 - f_b\right) dl_D \tag{27}$$

The combined bubble to emulsion gas interchange coefficients are evaluated by eq.(28):

$$0 = \left(\frac{1}{k_{bci}} + \frac{1}{k_{cei}} \right) - \frac{f_b}{K_{ti}} \tag{28}$$

For the evaluation of the bubble-cloud (k_{bci}) and cloud-emulsion (k_{cei}) gas interchange coefficients the expressions proposed by Kunii and Levenspiel [18] were adopted. The same method was used for the estimation of the heat interchange coefficient (H_t) [18].

The freeboard is simulated as an ideal two-phase PFR. The material balances of the gas and solid components in the freeboard are shown in eqs. (29) and (30), respectively:

$$\frac{1}{V_{F:\mathrm{RG}}}\frac{dF_{if}}{dl_F} = \varepsilon_f \sum_j^{\text{hom}o} \alpha_{ij} K_{Rjf} + \left(1-\varepsilon_f\right) \sum_j^{hete} \alpha_{ij} K_{Rjf} \tag{29}$$

$$\frac{1}{V_{F:\mathrm{RG}}}\frac{dF_{if}}{dl_F} = \left(1-\varepsilon_f\right) \sum_j^{hete} \alpha_{ij} K_{Rjf} \tag{30}$$

The energy balance for the freeboard is:

$$\frac{1}{V_{F:\mathrm{RG}}}\frac{dQ_f}{dl_F}=\varepsilon_f\sum_j^{\mathrm{hom}o}\left(-\Delta H_{Rj}\right)K_{Rjf}+\left(1-\varepsilon_f\right)\sum_j^{hete}\left(-\Delta H_{Rj}\right)K_{Rjf} \tag{31}$$

The ideal gas law is differentiated in terms of the gas enthalpy rate to evaluate the gas superficial velocity:

$$\frac{du_{gf}}{dl_F}=\frac{R_g}{A_{F:\mathrm{RG}}P_{F:\mathrm{RG}}\overline{cp}_{gf}}\frac{dQ_{gf}}{dl_F} \tag{32}$$

The derivative of the enthalpy of the gas phase is obtained by eq.(33), assuming that the heat capacity of the components is constant at each integration step:

$$\frac{dQ_{gf}}{dl_F}=\frac{Q_{gf}}{Q_f}\frac{dQ_f}{dl_F} \tag{33}$$

Simulation of Stripper and Slide Valves

The stripping volume and the material balance for the solids components were expressed through eqs.(34) and (35):

$$\frac{dV_{D:\mathrm{ST}}}{dt}=\frac{\dot{W}_{C:\mathrm{ST}}^{(l_D=1)}-\dot{W}_{C:\mathrm{ST}}^{(l_D=0)}}{\rho_p\left(1-\varepsilon_{mf}\right)} \tag{34}$$

$$\frac{dc_{i:\mathrm{ST}}}{dt}=\frac{\dot{W}_{C:\mathrm{ST}}^{(l_D=1)}\left(c_{i:\mathrm{ST}}^{(l_D=1)}-c_{i:\mathrm{ST}}\right)}{\rho_p\left(1-\varepsilon_{mf}\right)V_{D:\mathrm{ST}}} \tag{35}$$

The temperature of the catalyst stream at the exit of the regenerator standpipe (riser entrance) and at the exit of the liftline (regenerator entrance) was calculated by modeling the heat loss throughout their height with eq.(36):

$$\frac{dT}{dl}=\left(T_w-T\right)\frac{U_w\pi D_wL_w}{\dot{W}_Ccp_C} \tag{36}$$

The catalyst with concentration $c_{ie}^{(t)}$ enters the riser with rate that is determined by the slide valve at the end of the regenerator standpipe (eq.(37)):

$$\dot{W}_{C:\mathrm{RS}}=k_{\mathrm{SV_1}}\left(\frac{{A_{\mathrm{SP}}}^2{A_{t:\mathrm{SV_1}}}^2}{{A_{\mathrm{SP}}}^2-{A_{t:\mathrm{SV_1}}}^2}\right)^{0.5}\left(2\rho_p\left(1-\varepsilon_b\right)\left(P_{\mathrm{RG}}^{(l_F=1)}+\Delta P_{\mathrm{RG}}+\Delta P_{\mathrm{SP}}-P_{\mathrm{RS}}^{(l_F=1)}-\Delta P_{RS}\right)\right)^{0.5} \tag{37}$$

The same formulation is used to calculate the catalyst mass flow rate entering the regenerator:

$$\dot{W}_{C:\mathrm{RG}}^{(l_D=1)}=k_{\mathrm{SV_2}}\left(\frac{{A_{\mathrm{ST}}}^2{A_{t:\mathrm{SV_2}}}^2}{{A_{\mathrm{ST}}}^2-{A_{t:\mathrm{SV_2}}}^2}\right)^{0.5}\left(2\rho_p\left(1-\varepsilon_{mf}\right)\left(P_{\mathrm{ST}}^{(l_F=1)}+\Delta P_{\mathrm{ST}}-P_{\mathrm{RG}}^{(l_F=1)}-\Delta P_{\mathrm{LL}}\right)\right)^{0.5} \tag{38}$$

APPENDIX II: Hydrodynamic Correlations and Pressure Balance

Simulation of Riser

The weight hourly space velocity (*WHSV*) and the solids residence time (t_s) were calculated by eqs.(39) and (40), following the pilot riser geometry, that is divided in three regions:

$$0=\frac{\dot{W}_{F:\mathrm{RS}}}{\rho_p\left(V_{D:\mathrm{RS}}\left(1-\varepsilon_{D:\mathrm{RS}}\right)+V_{C:\mathrm{RS}}\left(1-\varepsilon_{C:\mathrm{RS}}\right)+V_{F:\mathrm{RS}}\left(1-\varepsilon_{F:\mathrm{RS}}\right)\right)}-\frac{WHSV}{3600} \tag{39}$$

$$0 = \frac{3600}{WHSV}\frac{\dot{W}_{F:\mathrm{RS}}}{\dot{W}_{C:\mathrm{RS}}} - t_{C:\mathrm{RS}} \tag{40}$$

(a) The mixing region at the riser bottom. The void fraction ($\varepsilon_{D:\mathrm{RS}}$) and subsequently the catalyst inventory of this region, were related to the superficial gas velocity by means of the empirical correlation of Richardson and Zaki [19] (eq.(41)), which substantiates for a dense regime in the bottom region of the pilot unit.

$$0 = \left(\frac{u_{g:D:\mathrm{RS}}}{u_{t:\mathrm{RS}}}\right)^{1/z} - \varepsilon_{D:\mathrm{RS}} \tag{41}$$

(b) The conical shaped intermediate region. Because of the very small volume of the intermediate region (15% of total riser volume), a simple approximation of averaged (between top and bottom regions) hydrodynamic attributes was used [20].

(c) The fast fluidization region at the riser top, which was simulated under the following assumptions: (i) the flow is fully developed, thus its hydrodynamic features remain constant with height; (ii) the total volumetric yield of the reaction is flowing through the whole height of this region; (iii) the particle acceleration is considered to be negligible. Hence, eq.(42) holds:

$$0 = \frac{u_{g:F:\mathrm{RS}}\rho_p A_{F:\mathrm{RS}}}{y_{F:\mathrm{RS}}\dot{W}_{C:\mathrm{RS}} + u_{g:D:\mathrm{RS}}\rho_p A_{F:\mathrm{RS}}} - \varepsilon_{F:\mathrm{RS}} \tag{42}$$

In eq.(42) $y_{F:\mathrm{RS}}$ is the average gas-solids slip factor for the top section of the riser, which was proven to play an important role in small diameter riser reactors [4]. The correlation of Pugsley and Berruti [20] was applied for the estimation of the gas-solids slip factor as shown in eq.(43), where Fr_g and Fr_t are the *Froude* numbers for the superficial gas velocity and solids terminal velocity, respectively:

$$0 = 1 + \frac{5.6}{Fr_{g:F:\mathrm{RS}}^2} + 0.47 Fr_{t:F:\mathrm{RS}}^{0.41} - y_{F:\mathrm{RS}} \tag{43}$$

A detailed pressure gradient analysis is required for small diameter risers [4]. For this analysis, all pressure gradients should be taken into account, and eq.(44) is valid where ΔP_{fg} is the gas-wall frictional pressure drop, ΔP_{fs} is the solids-wall frictional pressure drop, ΔP_{acc} is the pressure drop due to solids acceleration, and the other terms represent the pressure drop due to solids and gas static head throughout the total riser height:

$$\Delta P_{\mathrm{RS}} = \Delta P_{fg:\mathrm{RS}} + \Delta P_{fs:\mathrm{RS}} + \Delta P_{acc:\mathrm{RS}} + \varepsilon_{\mathrm{RS}}\rho_{g:\mathrm{RS}} g L_{\mathrm{RS}} + \left(1-\varepsilon_{\mathrm{RS}}\right)\rho_p g L_{\mathrm{RS}} \tag{44}$$

Simulation of Regenerator

For group A particles the emulsion gas superficial velocity is the gas velocity for zero net flow of solids, which equals the minimum bubbling velocity, plus (concurrent gas/solids flows) or minus (countercurrent gas/solids flow) the superficial solids velocity in the emulsion phase:

$$0 = u_{mb} \pm u_{se} - u_{ge} \tag{45}$$

For the evaluation of the minimum fluidization velocity the equation of Wen and Yu [18] is applied. For group A particles the minimum bubbling velocity, u_{mb}, is evaluated by the correlation of Abrahamsen and Geldart [21], which considers the effect of catalyst fines, f, on u_{mb}:

$$0 = \frac{2300\rho_{ge}^{\ 0.126}\mu_{ge}^{\ 0.523}\exp\left(0.716f\right)}{d_p^{\ 0.8} g^{0.934}\left(\rho_p - \rho_{ge}\right)^{0.934}} - \frac{u_{mb}}{u_{mf}} \tag{46}$$

The superficial gas velocity in the dense zone is then obtained by eq.(47):

$$0 = u_{gb} + u_{ge} - u_{g:\mathrm{RG}} \tag{47}$$

The fraction of the bubbles in the dense zone is:

$$0 = \frac{u_{gb}}{\upsilon_b} - f_b \tag{48}$$

The absolute bubble rise velocity υ_b is calculated as a function the isolated bubble rise velocity:

$$0 = 0.711\left(gd_b\right)^{0.5} + u_{g:\mathrm{RG}} - u_{ge} - \upsilon_b \tag{49}$$

The bubble diameter is estimated by the Wen-Mori correlation [18]:

$$0 = \exp\left(-\frac{0.3L_{D:\mathrm{RG}}l_D}{D_{D:\mathrm{RG}}}\right) - \frac{d_b^{(l_D=1)} - d_b}{d_b^{(l_D=1)} - d_b^{(l_D=0)}} \tag{50}$$

The initial bubble diameter and the maximum bubble diameter are estimated by eqs.(26) and (27), respectively:

$$0 = \frac{1.38}{g^{0.2}}\left(\frac{1}{1000}\left(u_{g:\mathrm{RG}}^{(l_D=0)} - u_{mb}\right)\right)^{0.4} - d_b^{(l_D=0)} \tag{51}$$

$$d_b^{(l_D=1)} = \min\left[0.652\left(A_{D:\mathrm{RG}}\left(u_{g:\mathrm{RG}}^{(l_D=1)} - u_{mb}\right)\right)^{0.4},\ 2\frac{\left(u_t^{(2.7d_p)}\right)^2}{g}\right] \tag{52}$$

The emulsion to freeboard elutriation rate K_i^* of a fraction of particles with average diameter d_{pi} is evaluated by the Zenz and Weil correlation [22]. The total entrainment rate K_t^* is then obtained by adding the rates of each respective fraction of particles. The catalyst density in the freeboard is a function of the gas-solids slip velocity, which is calculated on the basis of the correlation of Patience et al. [23], as shown in eq.(53):

$$0 = \frac{u_{gf}}{1 + 5.6/Fr_{gf} + 0.47Fr_t^{0.41}} - u_{sf} \tag{53}$$

The freeboard voidage is then calculated by eq.(54):

$$0 = 1 - \frac{K_t^*}{\rho_p u_{sf}} - \varepsilon_f \tag{54}$$

The pressure drop throughout the regenerator is calculated from the solids static head as shown in eq.(55):

$$\Delta P_{\mathrm{RG}} = \rho_p\left(1-\varepsilon_e\right)f_e g L_{D:\mathrm{RG}} + \rho_p\left(1-\varepsilon_f\right)gL_{F:\mathrm{RG}} \tag{55}$$

Simulation of Stripper and Slide Valves

The pressure drop throughout the stripper is calculated from the solids static head as shown in eq.(56):

$$\Delta P_{\mathrm{ST}} = \rho_p\left(1-\varepsilon_{mf}\right)gL_{D:\mathrm{ST}} \tag{56}$$

The catalyst circulation rate at the entrance and exit of the regenerator was correlated with the slide valves opening of the stripper and regenerator standpipes and the pressure drop by eq.(57) [24]:

$$\dot{W}_C = k_{\mathrm{SV}}\left(\frac{A_0^{\,2}A_{t:\mathrm{SV}}^{\,2}}{A_0^{\,2} - A_{t:\mathrm{SV}}^{\,2}}\right)^{0.5}\left(2\rho_p\left(1-\varepsilon\right)\Delta P_{SV}\right)^{0.5} \tag{57}$$

APPENDIX III: Nomenclature

A	cross-sectional area (m^2)
y_{c_x}	catalytic coke yield on feed basis (wt%)
y_c	total coke yield on feed basis (wt%)
D	diameter (m)
d_p	catalyst particle mean diameter (m^3)
cp	specific heat (kcal $mol^{-1}K^{-1}$)
E_x, E_c	activation energy of reaction to x, c (kcal mol^{-1})
f_b, f_e	bubble, emulsion phase volume fraction
F_{ib}	molar rate in bubble (mol s^{-1})
c_{ie}	molar concentration in emulsion (mol s^{-1})
F_{if}	molar rate in freeboard (mol s^{-1})
H_t	bubble-emulsion heat interchange (kcal m^{-3} s^{-1})
K_H	heat interchange rate group (kcal m^{-3} s^{-1})
K_{Mi}	mass interchange rate group (mol m^{-3} s^{-1})
K_{Rjb}	reaction rate group of reaction j - bubble phase (mol m^{-3} s^{-1})
K_{Rje}	reaction rate group of reaction j - emulsion phase (mol m^{-3} s^{-1})
K_{Rjf}	reaction rate group of reaction j - freeboard (mol m^{-3} s^{-1})
K_{SV1}, K_{SV2}	characteristic constant of slide valve SV1, SV2
K_{ti}	bubble-emulsion gas interchange coefficient (s^{-1})
k_x, k_c	pre-exponential factor of reaction to x or c
L	height (m)
l	dimensionless height
MW_F	feed molecular weight
n_x, n_c	catalyst decay exponent of reaction to x or c
Q_b	enthalpy rate in bubble phase (kcal s^{-1})
Q_C	enthalpy rate of catalyst (kcal s^{-1})
Q_{ge}	enthalpy rate of gas in emulsion phase (kcal s^{-1})
Q_{loss}	heat loss from the dense bed (kcal s^{-1})
P	pressure (Pa)
T	temperature (°C)
T_{RX}	riser reactor temperature (°C)
t_C	catalyst residence time (s)
t_{dead}	time lug in standpipe or liftline (s)
u_g	superficial gas velocity (m s^{-1})
u_t	catalyst particle terminal velocity (m s^{-1})
V	volume (m^3)
$WHSV$	weight hourly space velocity (hr^{-1})
$\dot{W}_C$	catalyst circulation rate (kg s^{-1})
$\dot{W}_F$	gas-oil feed rate (kg s^{-1})
y_x	gas-oil conversion on feed basis (wt%)
ΔH_{crack}	heat of catalytic cracking (kcal kg^{-1})
ΔH_{Rj}	heat of reaction j (kcal mol^{-1})

Greek Letters

α_{ij}	stoichiometric coefficient of component *i* in reaction *j*
ε_b	voidage of bulk catalyst
ε_{mf}	voidage at minimum fluidization
ε_e	dense bed emulsion void fraction
ε_f	freeboard void fraction
ε_r	riser void fraction
ρ_p	catalyst density (kg m^{-3})

Subscripts

g	gas phase
s	solids phase
b	bubble phase
e	emulsion phase
f	dilute phase

Unit Section Subscripts

D	dense phase or bottom section
C	cone intermediate section
F	dilute phase or top section
CY	regenerator cyclone
RS	riser
RG	regenerator
ST	stripper
SP	standpipe
LL	liftline